

Mechanism and Kinetics for the Initial Steps of Pyrolysis and Combustion of 1,6-Dicyclopropane-2,4-hexyne from ReaxFF Reactive Dynamics

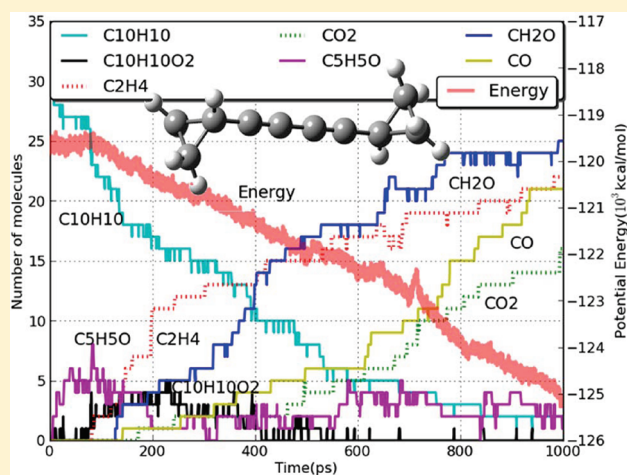
Lianchi Liu, Chen Bai, and Huai Sun*

School of Chemistry and Chemical Engineering, Shanghai Jiao Tong University, Shanghai 200240, China

William A. Goddard, III*

Materials and Process Simulation Center (139-74), California Institute of Technology, Pasadena, California 91125, United States

ABSTRACT: We report the kinetic analysis and mechanism for the initial steps of pyrolysis and combustion of a new fuel material, 1,6-dicyclopropane-2,4-hexyne, that has enormous heats of pyrolysis and combustion, making it a potential high-energy fuel or fuel additive. These studies employ the ReaxFF force field for reactive dynamics (RD) simulations of both pyrolysis and combustion processes for both unimolecular and multimolecular systems. We find that both pyrolysis and combustion initiate from unimolecular reactions, with entropy-driven reactions being most important in both processes. Pyrolysis initiates with extrusion of an ethylene molecule from the fuel molecule and is followed quickly by isomerization of the fuel molecule, which induces additional radicals that accelerate the pyrolysis process. In the combustion process, we find three distinct mechanisms for the O_2 attack on the fuel molecule: (1) attack on the cyclopropane ring expanding to form the cyclic peroxide which then decomposes; (2) attack onto the central single bond of the diyne which then fissions to form two C_5H_5O radicals; (3) attack on the alkyne-cyclopropane moiety to form a seven-membered ring peroxide which then decomposes. Each of these unimolecular combustion processes releases energy that induces additional radicals to accelerate the combustion process. Here oxygen has major effects both as the radical acceptor and as the radical producer. We extract both the effective activation energy and the effective pre-exponential factor by kinetic analysis of pyrolysis and combustion from these ReaxFF simulations. The low value of the derived effective activation energy (26.18 kcal/mol for pyrolysis and 16.40 kcal/mol for combustion) reveals the high activity of this fuel molecule.



1. INTRODUCTION

High-energy materials such as alkenes, alkynes, aromatics, nitrates,¹ and cyclics (e.g., JP-10²) are widely used as fuels or fuel additives for applications ranging from scramjets to pulse detonation engines.³ However, despite numerous experimental studies, considerable uncertainties remain regarding the molecular level chemical mechanisms underlying the shock ignition, pyrolysis, and combustion processes in these systems. Indeed, there is a need for a kinetic model based on a validated mechanism that could be used in macroscale simulations of these materials.^{4–8} Recently, a new high-energy density hydrocarbon material, 1,6-dicyclopropane-2,4-hexyne (Figure 1) (synthesized by adding cyclopropyl acetylene in isopropanol to catalytic cuprous chloride and tetramethylethylenediamine in isopropanol), has been introduced as a fuel or fuel additive for rockets and marine vessels.⁹ This potential fuel or fuel additive would help to ignite the fuel more easily to provide more energy in the ignition

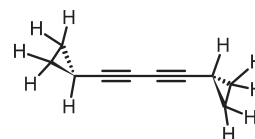


Figure 1. Structure of 1,6-dicyclopropane-2,4-hexyne.

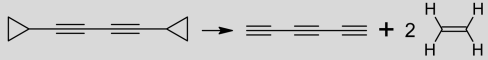
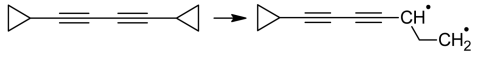
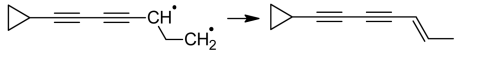
process. It is expected that this molecule is stable in the preheating injection so that it can provide more energy for both ignition and combustion compared with other possible fuel additives. Our main purpose here is to determine the chemical mechanisms underlying the pyrolysis and combustion. Is it stable

Received: November 1, 2010

Revised: December 16, 2010

Published: April 21, 2011

Table 1. Initial Reactions Observed in ReaxFF Unimolecular Pyrolysis^a

Name	Reactions	ΔE_{ReaxFF} (kal/mol)	ΔE_{QM} (kal/mol)	Observed Times
InitA		37.33	46.10	8
InitB		33.13	41.92	2
		-40.41	-54.79	

^a Reaction energies (kcal/mol) from ReaxFF and QM are compared.

enough in the preheating/injection process, and how would it help the ignition? Thus, it is most useful to understand:

- (1) the detailed initial mechanisms of pyrolysis and combustion of this material;
- (2) the kinetic parameters underlying its performance for pyrolysis and combustion; and
- (3) its mechanism as an ignition enhancer in kerosene or other regular fuels.

However, neither experimental nor theoretical studies have yet been published on these systems. In this work, we focus on the initial mechanism and kinetic analysis for both pyrolysis and combustion. Future studies will build upon these mechanistic studies to investigate its role as an additive in kerosene or other fuels.

For these studies, we use the ReaxFF reactive force field¹⁰ for RD, an approach that has been successfully used in condensed phases for up to millions of atoms with nanosecond time scale simulations to predict reasonable reaction mechanisms.¹¹ Recent applications of ReaxFF RD (reactive dynamics) include high impact decomposition of high-energy materials (cyclotetramethylene-tetranitramine (HMX),¹² triaminotrinitrobenzene (TATB),¹² cyclotrimethylenetrinitramine (RDX),^{13,14} pentaerythritol tetranitrate (PETN),¹⁵ and acetone peroxide (TATP)¹⁶), thermal decomposition of polydimethylsiloxane (PDMS),¹⁷ pyrolysis of kerogen precursors to form petroleum,¹⁸ and pyrolysis of lignite precursors to form coal.¹⁹

An alternative approach is to use ab initio molecular dynamics (AI-MD) for RD simulations of reacting systems in which the electronic wave function is calculated simultaneously with the motion of the nuclei (often referred to as Car–Parrinello MD). AI-MD has been useful for short reactive studies of small reactive molecules in condensed media (e.g., CH₃NO₂ for 15 ps). However, we are interested in following the important initial chemical processes in far larger reactive systems over a range of temperatures for periods of time of at least 10 ns. Thus, we use ReaxFF.

The ReaxFF force field has previously been applied successfully to provide accurate descriptions of the hydrocarbon oxidation process,²⁰ and it has been applied to the combustion kinetics of JP-10 hydrocarbon fuel.⁸ These successful applications of ReaxFF encouraged us to use ReaxFF for studying the pyrolysis and combustion of 1,6-dicyclopropane-2,4-hexyne, a promising system for which little detailed information is yet available.

Section 2 describes the details of various ReaxFF RD simulations. Section 3.1 discusses the detailed initial pyrolysis mechanisms for the unimolecular model obtained from a series of ReaxFF RD simulations. In addition, section 3.2 examines multimolecular pyrolysis in a series of ReaxFF RD simulations, which

are compared with the unimolecular pyrolysis. In sections 3.3 and 3.4, we investigate the unimolecular and multimolecular combustion of the fuel material with the appropriate ratio of O₂ to yield complete combustion. All unimolecular simulations, including both pyrolysis and combustion, were validated by comparing important reaction steps directly with quantum mechanics (QM). Finally, in section 3.5 we extract from the ReaxFF RD trajectories at various temperatures the rate and the activation energy for both pyrolysis and combustion of 1,6-dicyclopropane-2,4-hexyne.

2. MODELS AND METHODS

The RD simulations were carried out with the ReaxFF reactive force field,¹⁰ using the same potential functions and parameters from a recent ReaxFF RD study²⁰ of the initiation mechanisms and kinetics of pyrolysis and combustion of the JP-10 hydrocarbon Jet Fuel.⁸ This ReaxFF was initially developed to describe the chemistry of simple hydrocarbon molecules. The parameters were trained and then validated against QM results for important reactions.¹⁰ Further applications using ReaxFF include applications to high-energy materials, for which ReaxFF also proves to be consistent with reaction pathways observed in QM, being able to predict accurately the transition states in HMX,¹² TATB,¹² RDX,^{13,14} PETN,¹⁵ and TATP¹⁶ systems. For combustion systems, Chenoweth showed that the reactions between (C, H) and O containing systems are in good agreement with quantum calculations.²⁰ Furthermore, ReaxFF was used successfully to model/describe the JP-10 system,⁸ providing results in good comparison with experiments and QM calculations. We expect ReaxFF to be equally accurate for studying the pyrolysis and combustion processes in our fuel molecule.

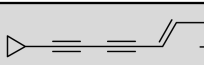
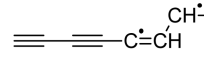
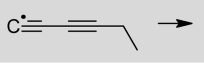
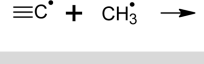
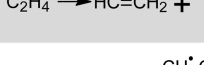
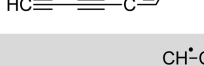


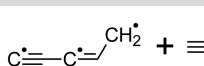
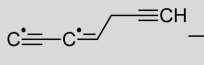
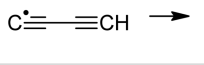
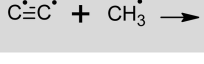
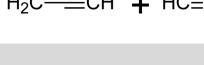

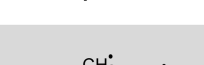

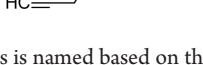
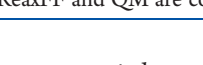
In addition, to further validate the results from RD calculations, we report QM calculations on intermediates in the reaction pathways observed in the RD simulations and compare the reaction step energies obtained from ReaxFF and QM. These QM calculations were calculated at the B3LYP/TZVP^{21,22} level of theory.

The RD simulations use NVT ensemble dynamics with periodic boundary conditions (PBC), with temperature control via a Berendsen thermostat²³ (damping constant = 0.1 ps). For each system, equilibrium calculations were first run at room temperature, and then the system was heated to the target temperature. During the equilibrium and heating process, the systems were calculated with fixed connectivity to prevent reactions from occurring.

To identify the fragments produced as a function of time during the simulations, we used a 0.3 bond order cutoff.

We used the PACKMOL package²⁴ to build the structural models.

Table 2. Specific Reactions Observed in Unimolecular Pyrolysis Simulations^b

Name ^a	Reactions	ΔE_{ReaxFF}	ΔE_{QM}	Product
B1_1		37.82	51.09	B1_int3
B1_2		149.60	149.97	B1_int4
B1_3		73.37	66.57	B1_int5
B1_4		-165.54	-130.24	B1_int6
B2_1		106.04	115.96	B2_int3
B2_2		-86.20	-76.28	B2_int3
B2_3		169.46	162.40	B2_int4
B2_4		81.20	93.36	B2_int5
B2_5		-156.34	-157.52	B2_int6
B2_6		24.93	60.75	B2_int7
B2_7		154.62	154.25	B2_int8
B2_8		-82.06	-110.08	B2_int9
B2_9		-143.53	-110.65	B2_int10
B2_10		-86.20	-76.28	B2_int11
A1_1		163.04	165.48	A1_int2
A1_2		-97.86	-60.62	A1_int3
A1_3		-87.01	-122.69	A1_int4
A1_4		46.13	89.65	A1_int5

^a The name of the reactions is named based on the initial reactions, i.e., A1_* refers to one reaction path following the initial reaction InitA. ^b Reaction energies (kcal/mol) from ReaxFF and QM are compared.

All the QM calculations were carried out with TURBOMOLE 5.8 package.²⁵

3. RESULTS AND DISCUSSION

3.1. Unimolecular Pyrolysis. The unimolecular pyrolysis simulations consider a single fuel molecule described using NVT ensemble dynamics with a cubic periodic cell with sides of 16.29 Å.

The system was first equilibrated at 300 K for 10 ps using a 0.1 fs time step and then heated to 2500 K at a uniform rate over a time of 10 ps. Finally, we carried out NVT RD for another 1 ns at 2500 K using a time step of 0.25 fs. This leads to a pressure of 84 MPa, which could be reached easily in the preheat/injection in engines.²⁶ To provide proper statistical sampling and an opportunity to observe a variety of mechanisms, we carried out 10 independent simulations of the unimolecular pyrolysis process.

Table 3. Reaction Energies (kcal/mol) for Initiation without Radicals (NoRad) in Unimolecular Pyrolysis

isomerization	ReaxFF	QM	molecular dissociation	ReaxFF	QM	molecule + molecule	ReaxFF	QM
InitA	37.33	46.10	B1_1	37.82	51.09	-		
InitB_1 ^a	33.13	41.92	A1_1	163.04	165.48	-		
InitB_2 ^a	-40.41	-54.79	A1_4	46.13	89.65	-		

^a Refers to the two-element reactions in InitB reactions.**Table 4. Reaction Energies (kcal/mol) for Initiation with Radical Production (YesRad) in Unimolecular Pyrolysis**

radical + radical	ReaxFF	QM	molecule + radical	ReaxFF	QM	radical dissociation	ReaxFF	QM
B1_4	-165.54	-130.24	A1_2	-97.86	-60.62	B1_2	149.60	149.97
B2_2	-86.20	-76.28				B1_3	73.37	66.57
B2_5	-156.34	-157.52				B2_3	169.46	162.40
B2_8	-82.06	-110.08				B2_4	81.20	93.36
B2_9	-143.53	-110.65				B2_6	24.93	60.75
A1_3	-87.01	-122.69				B2_7	154.62	154.25

From the ten independent simulations of pyrolysis with the unimolecular model, we observed two different initial decomposition reactions, as shown in Table 1.

- **InitA:** The initial reaction A involves ring opening of the cyclopropyl structures to produce two stable molecules: ethylene and 1,3,5-hexatriyne. This was observed 8 times for our 10 independent calculations.
- **InitB:** The initial reaction B starts with isomerization of the fuel molecule in which the cyclopropyl first opens to form a biradical intermediate which then transfers a hydrogen atom to form more stable intermediates. This was observed twice.

The reaction energy (ΔE_r) for InitA is positive (endothermic), while ΔE_r for InitB is negative (exothermic). However, InitA leads to a much larger increase in entropy (due to desorption of ethylene) than InitB, as evidenced by the increased preference for InitA at higher temperature.

In addition to these two initial reactions, we observed many other reactions in the unimolecular pyrolysis as listed in Table 2. The name of each elementary reaction reveals the lead initial reaction, with names of A* referring to the reactions following the initial reaction InitA and B* referring to the reactions following the initial reaction InitB. The reaction energies calculated by the ReaxFF RD method by QM are also listed in Table 2, showing that most ReaxFF energies are in good agreement with QM calculations. The exceptions are some radical decomposition reactions and radical–radical reactions, which seem to be due to underestimating the energy of radicals in ReaxFF. There are some differences in reaction energies, but these differences are mostly for high-energy situations in which radicals exist only for very short times. The trends in the total energy are consistent with the QM calculations, validating the accuracy of the ReaxFF force field.

Table 2 shows that InitB leads to much more complex reactions than InitA. Here, decomposition of the diyne structure and abstraction of hydrogen from ethylene are key reactions that start generating H, vinyl, ethynyl, and diyne radicals. These radicals are very reactive, leading to many new reactions that ultimately produce many additional stable molecules.

To analyze the various types of elementary reactions in the pyrolysis process, we classify the observed reactions into two groups (six different types):

- **NoRad:** no radicals contained in reactants (Table 3).

- **YesRad:** radicals are contained in the reactants (Table 4).

The tables show that the dissociation reaction energies for NoRad are positive (endothermic), leading to less active species, but with entropy release playing an important role in the pyrolysis. The reaction energies for the YesRad induced reactions (radical + radical and molecule + radical) are negative (exothermic), leading to reactive radicals which can lead to a variety of pyrolysis pathways.

Small species that we observed frequently include ethylene, 1,3,5-hexatriyne, C5 species (C_5H_4 , C_5H_3 , C_5H_2), and C3 species (C_3H_3 , C_3H_4), with the highest frequencies for ethylene and 1,3,5-hexatriyne.

To illustrate the energetics of the unimolecular pyrolysis, Figure 2 shows the relative energies (with the reactant as the reference state) for three of the ten pyrolysis simulations. Clearly the unimolecular pyrolysis reaction pathways are endothermic, showing the importance of entropy in the pyrolysis.

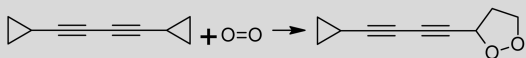
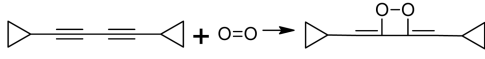
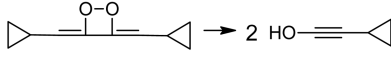
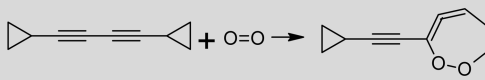
3.2. Multimolecular Pyrolysis. For multimolecular pyrolysis simulations, the thermal conditions were the same as for the unimolecular model. A periodic cubic box with 60 Å sides was built with 50 fuel molecules to achieve the same density as used in the unimolecular model. The system was first equilibrated at 300 K for 50 ps with a time step of 0.1 fs and then was heated to 2500 K at a uniform rate over another 10 ps. Then, we carried out RD for another 100 ps at 2500 K with a time step of 0.25 fs.

Fragment distributions and potential energy profiles with time for pyrolysis of the multimolecular system are presented in Figure 3, which shows the changes in the major products and intermediates in the process of pyrolysis with time at 2500 K. During the 100 ps simulation, ethylene (C_2H_4), C_2H radical, acetylene (C_2H_2), C_2 radical, and H_2 are the major products, while 1,3,5-hexatriyne (C_6H_2) is the major intermediate.

At the beginning of the pyrolysis, the number of fuel molecules decreases very quickly with the increase of ethylene and 1,3,5-hexatriyne. We find that the ratio of ethylene and 1,3,5-hexatriyne is about 2:1 in the first 10 ps. The concentration of 1,3,5-hexatriyne reaches a maximum at ~ 20 ps and gradually decreases in the remaining time. In the middle of the simulation, a large number of different radicals appear, with the major species being C_4H , C_2H , C_2H_3 , C_2 , and C_4H_2 , with other minor radicals shown in the figure.

Comparing with the unimolecular pyrolysis reactions in the last section, we see that the initial steps of multimolecular pyrolysis

Table 5. Initial Reactions Observed in Unimolecular Combustion^a

Name	Reactions	ΔE_{ReaxFF}	ΔE_{QM}	Times Observed
InitR1		-40.56	-28.42	3
InitR2		48.40	51.53	5
		-49.75	-38.26	
InitR3		-11.54	-8.17	2

^a Reaction energies (kcal/mol) from ReaxFF and QM are compared.

between (C, H) and O were turned off to prevent combustion reactions from occurring. Then we carried out 7 ns of RD at 1500 K using a 0.25 fs time step. The pressure of the system is about 80 MPa at 1500 K. Again, 10 parallel independent simulations were carried out to provide proper statistics and the opportunity for a variety of mechanisms to occur.

We examined unimolecular combustion at 1500 K because we established that no single fuel molecule decomposition occurs at this temperature during 10 ns simulations. This allows the study of the combustion reactions without complications of pyrolysis. From the ten independent simulations, Table 5 shows three different initial combustion reactions for the unimolecular model.

- **InitR2:** O₂ attacks the middle C–C bond of the diyne which then breaks immediately to form two C₅H₅O radicals. This was observed 5 times in our 10 independent simulations.
- **InitR1:** O₂ attacks the cyclopropyl structure to open the ring, forming a five-membered peroxide ring. This was observed 3 times in our 10 independent simulations.
- **InitR3:** O₂ attacks the cyclopropyl structure to open the ring, forming a 7-membered peroxide ring. This was observed 2 times in our 10 independent simulations

Clearly, InitR2 is an entropy-driven reaction, with the rate increasing with temperature.

Many other reactions following the initial reactions observed in the simulations are listed in Table 6. They are named based on the leading reaction as R1_*, R2_*, and R3_*. We see from the table that oxygen attack reactions and radical reactions dominate the subsequent reactions. Oxygen has a great effect on these reactions since it attacks the intermediates (especially the radicals) leading to subsequent products generally containing new radicals. Thus, the oxygen molecule plays the role of a radical acceptor to stabilize radical intermediates while also generating new radicals that subsequently can induce other radical reactions to accelerate the oxidation. In these initial reactions, high concentrations of small species observed are C₁₀H₁₀O₂, C₅H₅O radical, CO₂, CO, CH₂O, and many other C–O radicals.

Just as for pyrolysis, we classify the reactions into two groups (six different types):

- **NoRad:** no radicals contained in reactants (Table 7).
- **YesRad:** radical-containing reactions are involved (Table 8).

In contrast with pyrolysis, most reaction energies are negative (exothermic). Also, we find that some bimolecular reactions involve oxygen-related reactions.

To follow the energetics in unimolecular combustion, Figure 5 shows relative energies for the three different pathways of unimolecular combustion. We see that the combustion processes are all exothermic, indicating that combustion is far easier than pyrolysis. Here the close comparison between ReaxFF and QM reaction energies validates the accuracy of the ReaxFF force field. As with pyrolysis, the total energy trends are in good agreement with the QM calculations, but again ReaxFF seems to underestimate the energies of radicals.

3.4. Multimolecular Combustion. For multimolecular combustion simulations, we used 30 fuel molecules and 390 oxygen molecules in a cubic box of 62.0 Å side length. This leads to an equivalent ratio of $\Phi \approx 1.0$ and the same density as the unimolecular model. The box was first equilibrated at 300 K for 10 ps with a 0.1 fs time step and heated to 1500 K in 10 ps with a 0.25 fs time step using the NVT ensemble. In the equilibration and heating processes, the bond interactions between (C, H) and O were turned off to prevent combustion reactions from occurring. Then, RD at 1500 K was followed for 1 ns using 0.25 fs time steps.

Figure 6 presents the major product and intermediate distributions in 1 ns of multimolecular combustion simulations, where O₂ and other minor intermediates and products are omitted. This shows that the fuel molecules are nearly consumed in 1 ns of RD. The initial intermediates are C₁₀H₁₀O₂ and C₅H₅O, and the major products are CO₂, CO, CH₂O, and C₂H₄. The potential energy profile is also presented in Figure 6, showing that multimolecular combustion is exothermic.

Combustion in the multimolecular system leads to initial reactions similar to the unimolecular system, with most initial intermediates being C₁₀H₁₀O₂ and C₅H₅O. Table 6 shows that combustion of this fuel starts from oxygen attack at three possible attack positions. In addition, the major products CO₂, CO, and CH₂O are consistent with the unimolecular model. Nevertheless, multimolecular combustion is much more complex with many more radical intermediates appearing in the RD.

It is very interesting that a great deal of ethylene (C₂H₄) is generated in multimolecular combustion but not in unimolecular

Table 6. Specific Reactions Observed in Combustion Simulations^b

Name ^a	Reactions	ΔE_{ReaxFF} (kal/mol)	ΔE_{QM} (kal/mol)	Intermedi- ate Name
R1_1		-26.84	-15.92	R1_int2
R1_2		-39.14	-28.36	R1_int3
R1_3		61.88	52.94	R1_int4
R1_4		-19.61	-6.24	R1_int5
R1_5		-49.34	-50.13	
R1_6		-65.26	-57.16	R1_int6
R1_7		-26.26	-70.48	R1_int7
R1_8		-30.99	-9.45	R1_int8
R1_9		-21.55	-24.02	R1_int9
R1_10		-76.40	-91.14	R1_int10
R2_1		-50.45	-38.92	R2_int3
R2_2		-17.80	-36.97	R2_int4
R2_3		-33.24	-33.29	R2_int5
R3_1		-41.00	-22.21	R3_int2
R3_2		-84.31	-112.62	R3_int3
R3_3		-2.90	25.04	R3_int4
R3_4		7.40	-24.48	R3_int5
R3_5		-39.73	-41.81	R3_int6
R3_6		-15.46	-22.44	R3_int7
R3_7		-75.26	-88.05	R3_int8

^a The name of the reactions is based on the initial reactions; i.e., R1_* refers to one reaction path following the initial reaction InitR1. ^b Reaction energies (kcal/mol) from ReaxFF and QM are compared.

combustion. We find that the concentrations of C₈H₆ and C₆H₂ are quite minor in the combustion process. This shows that the C₂H₄ does not come from the pyrolysis of the fuel molecules but rather from radical reactions in the combustion process. This appearance of a great deal of ethylene in combustion of alkynes is

consistent with previous experimental and modeling studies²⁷ on the combustion of 1-butyne and 2-butyne.

In summary, combustion of 1,6-dicyclopropane-2,4-hexyne starts from the unimolecular oxidation with oxygen attacking any one of three different positions on the fuel molecule. This

Table 7. Reaction Energies (kcal/mol) for NoRad Unimolecular Combustion

isomerization	ReaxFF	QM	molecular dissociation	ReaxFF	QM	molecule + molecule	ReaxFF	QM
R1_6	−65.26	−57.16	R1_1	−26.84	−15.92	InitR1	−40.56	−28.42
			R1_3	61.88	52.94	R1_2	−39.14	−28.36
			R1_8	−30.99	−9.45	InitR2_1 ^a	48.40	51.53
			InitR2_2 ^a	−49.75	−38.26	R2_3	−33.24	−33.29
						InitR3	−11.54	−8.17
						R3_1	−41.00	−22.21
						R3_6	−15.46	−22.44

^a Refers to the two-element reaction of InitR2.

Table 8. Reaction Energies (kcal/mol) Classified for YesRad Unimolecular Combustion

radical + radical	ReaxFF	QM	molecule + radical	ReaxFF	QM	radical dissociation	ReaxFF	QM
R1_7	−26.26	−70.48	R1_4	−19.61	−6.24	R1_9	−21.55	−24.02
R1_10	−76.40	−91.14	R2_1	−50.45	−38.92	R2_2	−17.80	−36.97
R3_5	−39.73	−41.81	R3_2	−84.31	−112.62	R3_3	−2.90	25.04
R3_7	−75.26	−88.05				R3_4	7.40	−24.48

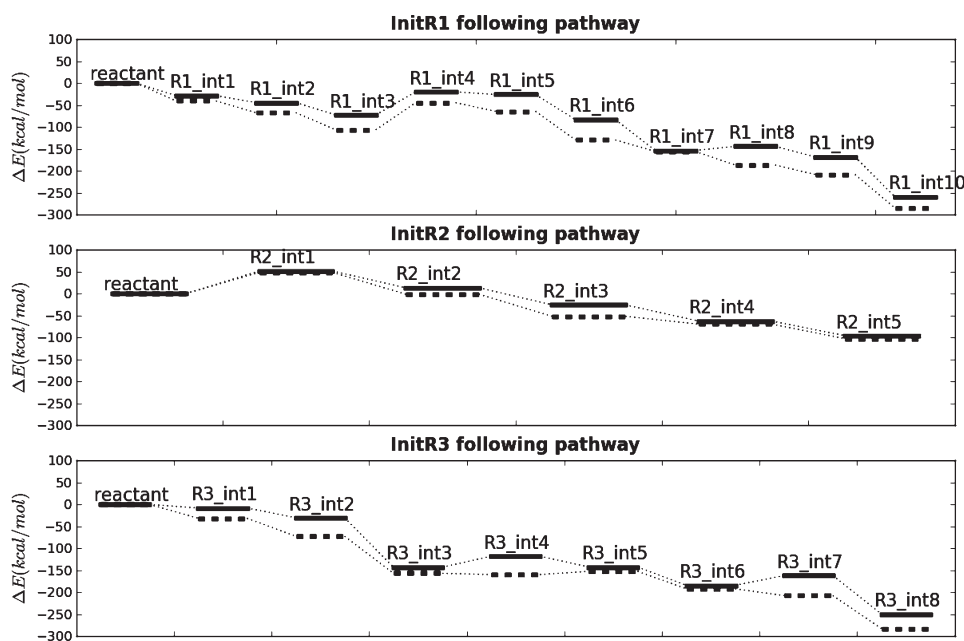


Figure 5. Relative energies of the three combustion pathways from ReaxFF RD. The solid line is the result of quantum chemistry calculation, and the dashed one is the result of ReaxFF calculation.

generates numerous radicals, making the combustion unstable toward explosion. Combustion generates numerous radicals, with many CO_2 , CH_2O , and CO generated from the initial or radical reactions, while a number of C_2H_4 are generated only from subsequent radical reactions.

The major product distributions as a function of temperature are presented in Figure 7. We see that the concentrations of CH_2O , CO_2 , and C_2H_4 are not sensitive to temperature, while the concentrations of H_2O , H_2 , and CO increase with increasing temperature. This indicates that increased radical reactions occur at high temperature, especially the destruction of hydrogen radicals and the oxygen-related reactions.

Comparing with the pyrolysis process, the combustion temperature is much lower, and the process is much faster. Exothermic

combustion is much faster than endothermic pyrolysis. The reactions of both pyrolysis and combustion start from the unimolecular reactions, and the unimolecular pyrolysis/combustion generates many radicals to accelerate the pyrolysis/combustion process.

3.5. Kinetic Analysis of Pyrolysis and Combustion. To investigate the kinetic properties for pyrolysis and combustion, we carried out RD on the multimolecular models of pyrolysis and combustion for several temperatures. We used the range of 1600–2500 K in 100 K steps for the pyrolysis kinetic analysis and the range of 1500–2000 K in 100 K steps for the combustion model. These simulations were carried out for 100 ps at each temperature with a 0.25 fs time step for the pyrolysis model and for 1 ns with a 0.25 fs time step for the combustion model.

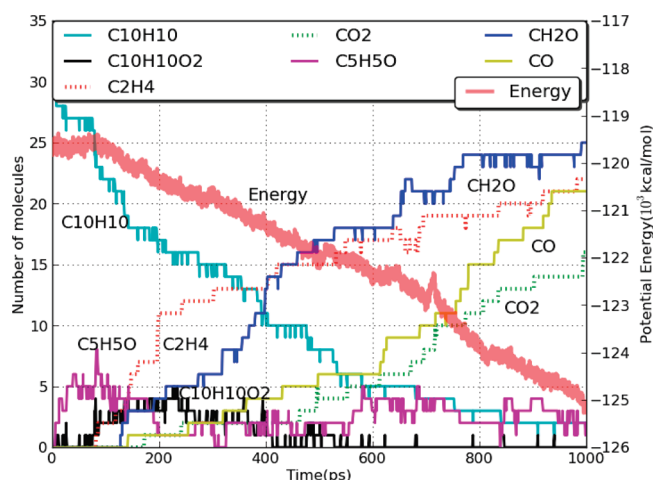


Figure 6. Fragment distributions and potential energy profile of multi-molecular combustion at 1500 K in 0.1 ps increments.

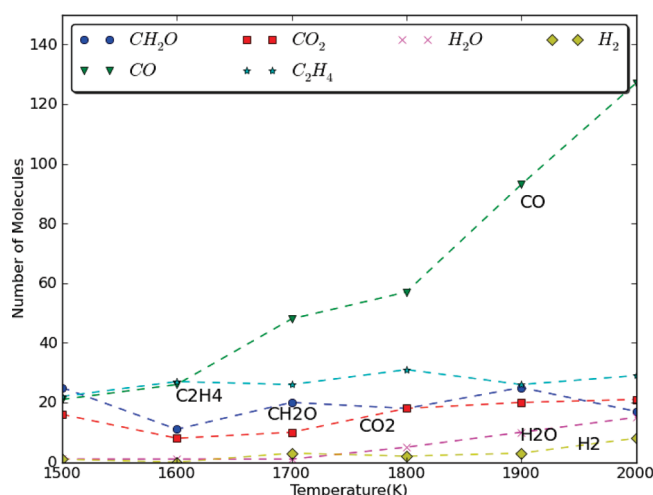


Figure 7. Product distributions at the end of 1 ns RD combustion as a function of temperature.

The log of the initial rate of the loss of fuel molecules is plotted versus $(1/T)$ in Figure 8 for both pyrolysis and combustion. We observe first-order kinetics that are fit reasonably well to a single Arrhenius function, allowing us to extract an effective activation energy E_a and pre-exponential factor A .

Figure 8 shows that pyrolysis of 1,6-dicyclopropane-2,4-hexyne leads to $E_a(\text{pyr}) = 26.18$ kcal/mol, which can be compared to the 0 K endothermicity from ReaxFF of 37.33 kcal/mol for the NoRad process of direct abstraction of one ethylene from the fuel molecule and 37.82 kcal/mol for abstraction of ethylene from the fuel molecule after the isomerization. We would expect the temperature change in ΔH to be $\Delta C_p^* T$ or $4RT$ which would lead to $\delta\Delta H = 19.87$ kcal/mol at 2500 K, leading to a total of ~ 57 kcal/mol. This is 1.2 times larger than observed, suggesting that the decompositions are not fully unimolecular.

The pre-exponential factor derived from the pyrolysis simulations is $A = 7.38 \times 10^{11}$. Assuming unimolecular decomposition, transition state theory leads to $A = (k_B T/h) \exp(\Delta S^\ddagger/R)$ where $\Delta S^\ddagger = -5.43$ eu. This negative activation of entropy is consistent with the TST for multimolecular reactions, suggesting that the reaction involves a multimolecular transition state. This

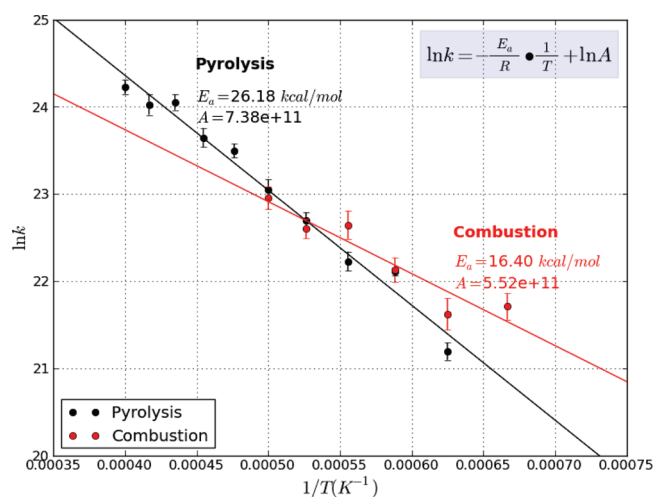


Figure 8. Kinetic analysis of pyrolysis and combustion. Black is for the pyrolysis, and red is for the combustion. The activation energy of pyrolysis and combustion is 26.18 and 16.40 kcal/mol, respectively, and the pre-exponential factors of pyrolysis and combustion are 7.38×10^{11} and 5.52×10^{11} , respectively.

pre-exponential factor combines unimolecular decomposition (that could be treated with RRKM theory), collisional activation, and the effective entropy change for the typical decomposition.

For combustion of 1,6-dicyclopropane-2,4-hexyne, Figure 8 leads $E_a(\text{comb}) = 16.40$ kcal/mol, with a pre-exponential factor of $A = 5.52 \times 10^{11}$. We expect a lower E_a for combustion since O_2 can stabilize the initial steps of bond breaking and since the initial reaction steps are far more exothermic. We can compare the E_a to the initial reaction step at 0 K of InitR1, InitR2, and InitR3 for the three different oxygen-attack positions. Correcting for temperature, this would lead to -2.19 kcal/mol at 1500 K. Assuming TST, we can extract $\Delta S^\ddagger = -10.29$ eu, which shows the decrease of entropy at the transition state because of the oxygen attack.

4. CONCLUSION

We have investigated the initial mechanisms of pyrolysis and combustion of the 1,6-dicyclopropane-2,4-hexyne fuel molecule using ReaxFF RD.

For pyrolysis, we find that the endothermic, entropy-driven abstraction of ethylene from the fuel molecule is the most important initial step. We also observe isomerization of the fuel molecule as an occasional initial reaction (20%). Although not the main reaction, this latter mechanism produces radicals that have a great effect on multimolecular pyrolysis. Briefly, the pyrolysis process starts from the unimolecular decomposition and isomerization, and the generated radicals accelerate the subsequent pyrolysis reactions. We find that C_6H_2 is an important intermediate and that major products from 100 ps RD are C_4H , C_2H , C_2H_3 , C_2 , and C_4H_2 .

Combustion occurs from three different initial oxygen-attack reactions.

1. **InitR2:** O_2 attack on the C–C single bond of the diyne is preferred. This entropy-driven combustion starts from unimolecular oxidation, generating many radical species, and leading to explosive combustion. In this process, oxygen serves both as a radical acceptor and as a radical producer, which dramatically increases the combustion rates. Major products observed in 1 ns simulations are CO_2 ,

CH₂O, CO, and C₂H₄. Here we found ethylenes generated from the radical reaction but not the pyrolysis attack on the cyclopropane ring, expanding to form the cyclic peroxide.

2. **InitR1**: O₂ attacks the cyclopropyl structure to open the ring forming a five-membered peroxide ring.
3. **InitR3**: O₂ attacks the cyclopropyl structure to open the ring forming a seven-membered peroxide ring.

The effects of temperature on pyrolysis and combustion were considered. Here we found that at high temperature more radicals would be generated and that H abstractions are sensitive to the temperature.

Activation energy and pre-exponential factor of pyrolysis and combustion were obtained from the kinetic analysis. The activation energies of pyrolysis and combustion are very low, making both pyrolysis and combustion fast.

In addition, the reaction energies of unimolecular models were validated by the QM method, and the consistent results show that the ReaxFF force field is very accurate for investigating the pyrolysis and combustion process.

This success in using a previously derived ReaxFF to study the pyrolysis and combustion of a new fuel validates this ReaxFF approach for designing new fuels, perhaps to reduce the sensitivity while maintaining high exothermicity.

AUTHOR INFORMATION

Corresponding Author

*E-mail: wag@wag.caltech.edu; huaisun@sjtu.edu.cn.

ACKNOWLEDGMENT

We thank Jonathan E. Mueller for helpful discussions and comments. Financial support from the National Science Foundation of China (No. 20473052), NSAF funding (No. 10676021), and National Basic Research Program of China (No. 2003-CB615804 and 2007CB209701) is gratefully acknowledged. We acknowledge the funding from China Scholarship Council (No. 2009623057). Funding from ONR (N00014-09-1-0634) and ARO-MURI (W911NF-08-1-0124 and W911NF-05-1-0345) and Los Alamos National Labs. is acknowledged.

REFERENCES

- (1) Zhang, F. A.; R.; Thibault, P. A.; Murray, S. B. *Shock Waves* **2001**, 10 (6), 457–466.
- (2) Li, S. C. V.; B.; Williams, F. A. *AIAA J.* **2001**, 39 (12), 2351–2356.
- (3) Roy, G. D.; Frolov, S. M.; Borisov, A. A.; Netzer, D. W. *Prog. Energy Combust. Sci.* **2004**, 30 (6), 545–672.
- (4) Tishkoff, J. M. D., J.P.; Edwards, T. In *Future directions of supersonic combustion research: Air Force/NASA Workshop on Supersonic Combustion*, paper AIAA 97-1017, 1997.
- (5) Lindstedt, P. In *Modeling of the Chemical complexities of flames. Twenty-Seventh Symposium (International) on Combustion/The Combustion Institute*, 1998; pp 269–285.
- (6) Simmie, J. M. *Prog. Energy Combust. Sci.* **2003**, 29 (6), 599–634.
- (7) William, F. A. In *Short chemical mechanisms for deflagration and detonations. Western States Section/The Combustion Institute Spring Meeting* 2004, 2004.
- (8) Chenoweth, K.; van Duin, A. C. T.; Dasgupta, S.; Goddard, W. A., III. *J. Phys. Chem. A* **2009**, 113 (9), 1740–1746.
- (9) Suri, S. C.; Tinnirello, M. G. Synthesis of 1,4-dicyclopentyl-1,3-butadiyne. US7217851-B1, 15 May 2007 C07C-004/00 200741, 2007.
- (10) van Duin, A. C. T.; Dasgupta, S.; Lorient, F.; Goddard, W. A. *J. Phys. Chem. A* **2001**, 105 (41), 9396–9409.
- (11) Nakano, A.; Kalia, R.; Nomura, K.; Sharma, A.; Vashishta, P.; Shimojo, F.; van Duin, A.; Goddard, W.; Biswas, R.; Srivastava, D. *Comput. Mater. Sci.* **2007**, 38, 642.
- (12) Zhang, L.; Zybin, S. V.; van Duin, A. C. T.; Dasgupta, S.; Goddard, W. A.; Kober, E. M. *J. Phys. Chem. A* **2009**, 113 (40), 10619–10640.
- (13) Strachan, A.; van Duin, A. C. T.; Chakraborty, D.; Dasgupta, S.; Goddard, W. A. *Phys. Rev. Lett.* **2003**, 91 (9), 098301.
- (14) Alejandro, S.; Edward, M. K.; Adri, C. T. v. D.; Jonas, O.; William, A. G., III. *J. Chem. Phys.* **2005**, 122 (5), 054502.
- (15) Oleynik, I. I.; Conroy, M.; Zybin, S. V.; Zhang, L.; Duin, A. C. v.; W., A. G., III; White, C. T. *AIP Conf. Proc.* **2006**, 845, 573–576.
- (16) vanDuin, A. C. T.; Zeiri, Y.; Dubnikova, F.; Kosloff, R.; Goddard, W. A. *J. Am. Chem. Soc.* **2005**, 127 (31), 11053–11062.
- (17) Chenoweth, K.; Cheung, S.; vanDuin, A. C. T.; Goddard, W. A.; Kober, E. M. *J. Am. Chem. Soc.* **2005**, 127 (19), 7192–7202.
- (18) Salmon, E.; van Duin, A. C. T.; Lorient, F.; Marquaire, P.-M.; Goddard, W. A., III. *Org. Geochem.* **2009**, 40, 1195–1209.
- (19) Salmon, E.; van Duin, A. C. T.; Lorient, F.; Marquaire, P.-M.; Goddard, W. A., III. *Org. Geochem.* **2009**, 40, 416–427.
- (20) Chenoweth, K.; vanDuin, A. C. T.; Goddard, W. A. *J. Phys. Chem. A* **2008**, 112 (5), 1040–1053.
- (21) Schafer, A.; Huber, C.; Ahlrichs, R. *J. Chem. Phys.* **1994**, 100, 5829.
- (22) Unterreiner, B.; Sierka, M.; Ahlrichs, R. *Phys. Chem. Chem. Phys.* **2004**, 6, 4377.
- (23) Berendsen, H. J. C.; Postma, J. P. M.; van Gunsteren, W. F.; DiNola, A.; Haak, J. R. *J. Chem. Phys.* **1984**, 81 (8), 3684.
- (24) Martínez, L.; Andrade, R.; Birgin, E. G.; Martínez, J. M. *J. Comput. Chem.* **2009**, 30 (13), 2157–2164.
- (25) Ahlrichs, R.; Bär, M.; Häser, M.; Horn, H.; Kölmel, C. *Chem. Phys. Lett.* **1989**, 162 (3), 165.
- (26) Lee, C.; Park, S.; Kwon, S. *Energy Fuels* **2005**, 19, 2201.
- (27) Belmekki, N.; Glaude, P. A.; Costa, I. D.; Fournet, R.; Battin-Leclerc, F. *Int. J. Chem. Kinet.* **2002**, 34 (3), 172–183.